In vitro characterization and rational analog design of a novel inhibitor of telomerase assembly in MDA MB 231 breast cancer cell line

ROMINA ARMANDO[1], MAIA CABRERA[2], ROMAN VILARULLO[1], PATRICIO CHINESTRAD[2], JULIAN MAGGIO[1], CAMILA PADERTA[1], PABLO LORENZANO MENNA[2], DANIEL GOMEZ[1*] and DIEGO MENGUAL GÓMEZ[1*]

[1]Molecular Oncology Unit, Center of Molecular and Translational Oncology, Quilmes National University, Bernal, Buenos Aires B1876BXD; [2]Laboratory of Molecular Pharmacology, Quilmes National University, Bernal, Buenos Aires B1876BXD, Argentina

Received May 13, 2022; Accepted August 17, 2022

DOI: 10.3892/or.2022.8403

Abstract. Tumor cells have unlimited replicative potential, principally due to telomerase activity, which requires assembly of components such as dyskerin (hDKC1), human telomerase reverse transcriptase and human telomerase RNA (hTR). The present study aimed to develop novel inhibitors of telomerase to target the interaction between hTR and hDKC1. Based on docking-based virtual screening, the candidates R1D2-10 and R1D2-15, which exert an *in vitro* inhibitory effect on telomerase activity, were selected. Human mammary adenocarcinoma MDA-MB 231 cell line was selected to evaluate the treatment with the aforementioned compounds; the effect on telomere length was evaluated by qPCR, where both compounds caused telomere shortening. Furthermore, expression of genes related to apoptosis and senescence process, as well SA β galactosidase staining and caspase 3 activity. We determine that only compound R1D2-10 showed and effect on the induction of these cellular processes. To identify a lead compound from R1D2-10, 100 analogs were designed by LigDream server and then analyzed by AutoDock Vina and Protein-Ligand Interaction Profile to calculate their docking energy and target interaction. Those with the best values and specific residue interactions were selected for *in silico* prediction of absorption, distribution, metabolism, excretion (ADME), off-target interaction, toxicity and chemical diversity. A total of nine chemically different analogs was identified with higher docking affinity to the target, suitable ADME properties and not off-target interaction and side effects. These results indicated R1D2-10 and its analogs may serve as potential novel inhibitors of telomerase and antitumoral drugs in clinical use.

Correspondence to: Dr Romina Armando, Molecular Oncology Unit, Center of Molecular and Translational Oncology, Quilmes National University, 352 Roque Saenz Peña, Bernal, Buenos Aires B1876BXD, Argentina
E-mail: romina.armando@unq.edu.ar

*Contributed equally

Key words: dyskerin, telomerase, human telomerase RNA, breast cancer, analog design, absorption, distribution, metabolism, excretion properties, chemical diversity

Introduction

Telomerase is one of the primary targets for developing effective therapies against cancer due to its expression in most types of tumor, as well as in stem-like tumor cells. As is shown in Fig. 1, several strategies were designed to attack positive telomerase cells, by targeting different sites of the proteins involved in telomere homeostasis. Additionally, normal cells-including stem cells-have lower telomerase activity and generally maintain telomeres at longer lengths in comparison to tumor cells. These properties confer a benefit that ensures minimum risk for possible telomere shortening in stem cells, making telomerase a selective target to cancer cells (1).

Based on experimental evidence that links telomeric homeostasis with drug resistance and antitumor treatment (2,3), the development of drugs targeting telomerase represents a promising tool for antitumor therapy, both alone and in combination with other treatment. For example, the treatment with 6-thio-2'deoxyguanosine (6-thio-dG), a telomerase substrate precursor analogue, it is reported as a novel and effective strategy to treat therapy-resistant melanoma, pediatric brain tumors and Non-Small Cell Lung Cancer (NSCLC) (4-6). Furthermore, Wu *et al* proposed a nanoplatform containing the specific telomerase inhibitor BIBR1532 as a strategy to reverse multidrug resistance in breast cancer (7). The telomerase complex is regulated at multiple levels, by mechanisms such as epigenetic regulation, transcriptional and post-translational processing, intracellular compartmentalization, recruitment and substrate accessibility (2). Considering these processes, different strategies have been adopted to develop novel telomerase inhibitor therapies that recognize TERT tumour-associated antigens; small molecule inhibitors or oligonucleotides that suppress telomerase activity; disruptors of telomerase regulation or function such as G-quadruplex stabilizers; targeting TERT gene expression and utilization of nucleoside analogues to disrupt elongation of newly extended

telomeres (8,9). The primary aim of antitumor therapy targeting telomerase is to selectively induce tumor cell death without affecting healthy cells (10).

Active human telomerase is a ribonucleoprotein comprising catalytic subunit (human telomerase reverse transcriptase (hTERT) and template RNA human telomerase RNA (hTR) (11). However, other proteins are necessary for *in vivo* assembly, subcellular trafficking and telomere recruitment of the functional telomerase holoenzyme. Among these proteins, dyskerin (hDKC1), which allows correct assembly and stabilization of mature hTR, is essential for telomerase activity (11).

Our previous study designed a novel strategy for rational development of new holoenzyme telomerase assembly inhibitors based on interruption of the interaction between hDKC1 and hTR. An *in silico* approach was used to obtain a model of hDKC1 with accurate model parameters (confidence score, template modelling score, root mean square deviation and stereochemical property) to identify candidate compounds with inhibitory effects on telomerase activity by docking-based virtual screening (DBVS) (11). The present study aimed to characterize the effect of two of these candidates: R1D2-10, a carboxy-phenyl-benzamide, and R1D2-15, an indoquinoline. Both compounds showed greatest telomerase inhibition at the lowest concentration. Here, a breast cancer model was selected to validate these candidates as telomerase is a potential target for diagnosis and therapy in breast cancer (12). MDA MB 231 breast cancer cell line was previously used (11) to determine the effect of these compounds on telomere shortening, senescence and apoptosis; the aforementioned study determined that R1D2-10 showed the best performance as a telomerase inhibitor. The present study aimed to identify novel drugs with potential clinical use for cancer treatment. Analogs of the parental compound R1D2-10 were designed and interaction with the target, as well as absorption, distribution, metabolism, excretion (ADME) properties, toxicity, off-target interaction, and chemical diversity were assessed.

Materials and methods

Drug preparation. R1D2-10 and R1D2-15 lyophilized compounds (10 mg) were purchased from Enamine LTD, Ukraine. Each compound was solubilized in sterile DMSO within a laminar flow to obtain 10 mM stock solution.

Breast cancer cell lines. Breast cancer is a complex and heterogenous disease classified into at least five subtypes: Luminal A and B, human epidermal growth factor receptor 2, basal and normal (13). To represent subtypes three breast cancer cell lines were selected: Human mammary adenocarcinoma MDA MB 231, which is a highly aggressive, invasive and poorly differentiated claudin-low triple-negative breast cancer model; MDA MB 468, which is less aggressive and belongs to basal type and MCF-7, a poorly-aggressive and non-invasive Luminal A subtype.

Culture conditions. All cell lines were obtained from the American Type Culture Collection (cat. nos. HTB-26, HTB-132 and HTB-22). Cells were grown in DMEM (Thermo Fisher Scientific, Inc.) supplemented with 10% heat-inactivated FBS (Sigma-Aldrich; Merck KGaA), 2 mM glutamine and 80 μg/ml gentamicin at 37˚C in 5% CO_2 atmosphere. Cell cultures were routinely sub-cultured by trypsinization according to the manufacturer's instructions. For MDA MB 468 culture, Gibco MEM-Non-essential amino acids 100X (Thermo Fisher Scientific, Inc.) was added to the medium to a final concentration of 1X. DMSO was used as a vehicle. Mycoplasma testing was performed for the cell lines by Indirect HoechstStain (cat. no. 62249, Thermo Fisher Scientific, Inc.), according to the manufacturer's instructions.

Cell proliferation assay. MDA MB 231, MDA MB 468 and MCF-7 cells ($1x10^4$) were plated in 96-well plates. After 24 h, cells were treated with different concentrations of compound R1D2-10 or R1D2-15 (0.0,3.1,6.3,12.5,25.0,50.0 μM) for 72 h at 37˚C. Cell survival was measured by colorimetric MTT assay (Sigma-Aldrich; Merck KGaA). Formazan was dissolved in DMSO and the plate was read at 570 nm in a microplate reader. The concentration producing 50% inhibition (IC_{50}), maximmum response (E_{max}) and goodness of fit (R^2) values were determined by non-linear regression function of GraphPad Prism 6® (GraphPad Software, Inc.). A total of of three independent experiments was performed.

Determination of telomerase activity. Telomerase activity was determined by real-time quantitative telomerase repeat amplification protocol (RQ-TRAP) assay using SYBR-Green (StepOne™ System; Thermo Fisher Scientific, Inc.). MDA MB 231, MDA MB 468 and MCF-7 cells in logarithmic growth phase were harvested and washed once with PBS. Cells ($2x10^6$) were transferred to 1.5 ml conical tubes and centrifuged for 8 min at 450 x g at room temperature. The pellet was lysed with 200 μl 3-[(3-Cholamidopropyl) dimethylammonio]-1-propanesulfonate buffer 0.5% p/v with RNaseOUT (Thermo Fisher Scientific, Inc.) and protease inhibitor (Sigma-Aldrich; MercK KGaA), quantified by Micro BCA Protein Assay (Thermo Fisher Scientific, Inc.) according to the manufacturer's instructions and stored at -20˚C until use. RQ-TRAP assay was performed in a final volume of 10 μl, using 2 μl lysate as a template, Power SYBR Green Master Mix 1X (Thermo Fisher Scientific, Inc.), 250 nM alternative complementary primer (5'-GCGCGGCTTACCCTTACCCTT ACCCTAACC-3') and 800 nM telomerase substrate primer (5'-AATCCGTCGAGCAGAGTT-3'). Following 20 min incubation at 25˚C, thermocycling conditions were as follows: Initial denaturation at 90˚C for 10 min, followed by 40 cycles of 95˚C for 15 sec and 60˚C for 10 sec. The reaction ended with melt curve analysis in which the temperature was increased from 55 to 95˚C at a linear rate of 0.2˚C/sec. StepOne Software v2.3 (Thermo Fisher Scientific, Inc.) was used to analyze results.

Relative telomere length determination. Telomere length was determined as described by Cawthon (14). According to the manufacturer's instructions, high molecular weight DNA from control (DMSO) and treated MDA MB 231 cells was extracted using Pure gDNA kit (Productos Bio-Lógicos). Extracted DNA was quantified at 230, 260 and 280 nm absorbance using NanoDrop 1000 (Thermo Fisher Scientific, Inc.) spectrophotometer. Specific primers for the repetitive telomere sequence were used to quantify telomere length. Specific primers for

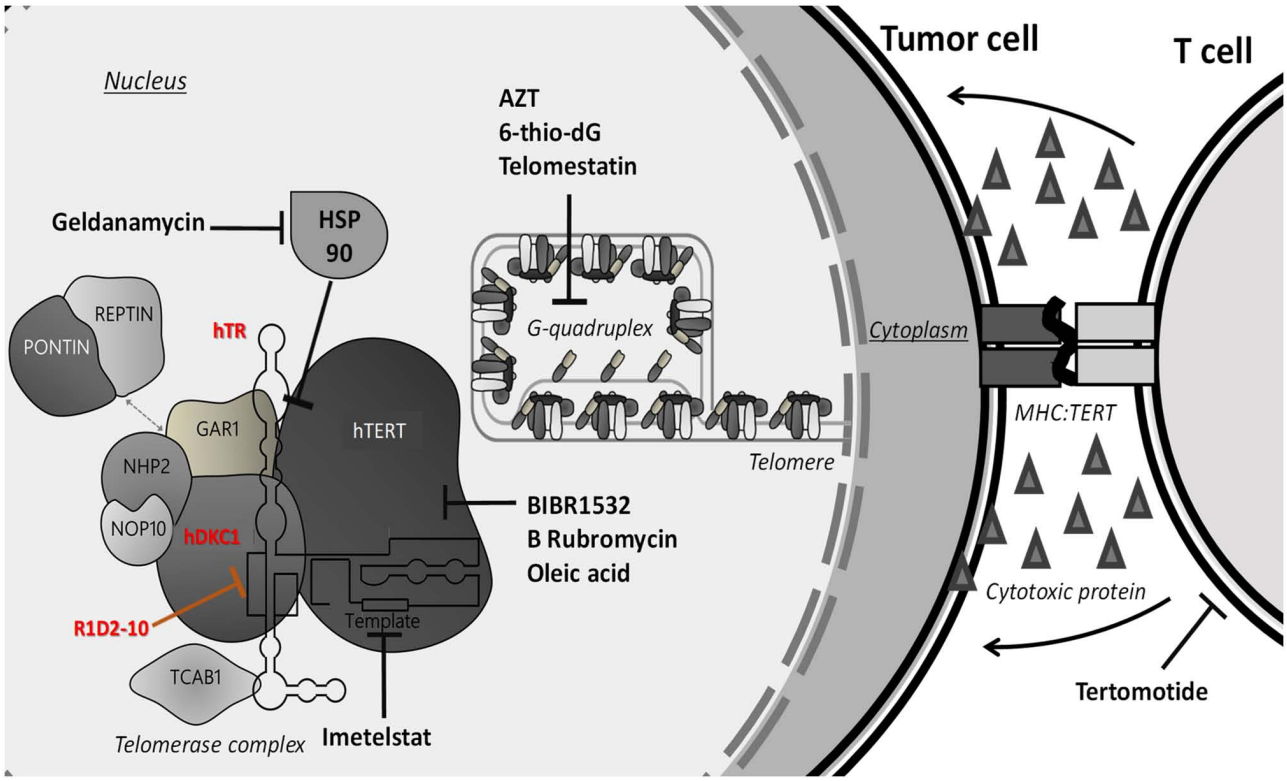

Figure 1. Telomerase inhibition approaches. Strategies designed to inhibit telomerase by targeting sites of proteins involved in telomere homeostasis. Red, action site of compound R1D2-10. HSP, heat shock protein; REPTIN, RuvB like AAA ATPase 2; PONTIN (RuvB like AAA ATPase 1); hTR, human telomerase RNA; hTERT, human telomerase reverse transcriptase; hDKC1, dyskerin; TCAB1, telomerase cajal body protein 1 homolog; AZT, azidothymidine; HLA, human leukocyte antigen.

the single copy gen ribosomal protein lateral stalk subunit P0 (rplp0) were used to determine the genome copies on the sample. Primer sequences and concentrations were as follows: Telomere length (500 nM) forward, 5'-CGGTTTGTTTGG GTTTGGGTTTGGGTTTGGGTTTGGGTT-3' and reverse, 5'-GGCTTGCCTTACCCTTACCCTTACCCTTACCCTTAC CCT-3' and single copy gen *rplp0* (250 nM) forward, 5'-CAG CAAGTGGGAAGGTGTAATCC-3' and reverse, 5'-CCC ATTCTATCATCAACGGGTACAA-3'. The PCR thermocycling conditions were as follows: Initial denaturation at 90˚C for 10 min, followed by 40 two-step PCR cycles at 95˚C for 15 sec and 60˚C for 10 sec. Results were analyzed using v2.3 StepOne® software (Thermo Fisher Scientific, Inc.).

RNA extraction and copy DNA synthesis. Total RNA was extracted from control (DMSO) and treated MDA MB 231 cells using Bio-Zol (Productos Bio-Lógicos) according to the manufacturer's instructions. The extracted RNA was quantified at 230, 260, and 280 nm absorbance using NanoDrop 1000 (Thermo Fisher Scientific, Inc.) spectrophotometer. DNA was synthesized from 1 μg total RNA in 20 μl reaction mix using oligodT18 (PB-L) and Superscript III (Thermo Fisher Scientific, Inc.) according to the manufacturer's instructions.

Evaluation of senescence. Senescence was evaluated in control (DMSO) and MDA MB 231 cells treated with R1D2-10 and R1D2-15. Differential expression of replicative senescence-associated genes, such as *glb1* (galactosidase β1) and *p16ink4a* (cyclin-dependent kinase inhibitor 2A), was evaluated by qPCR (ΔΔCq method) (15) using SYBR-Green (StepOne™ System; Thermo Fisher Scientific, Inc.). Primer sequences were as follows: G*lb1* (900 nM) foward, 5'-CCA CGATCGAGCATATGTTG-3' and reverse, 5'-CAGAGTGGC TCCAGCTTTC-3' and *p16ink4a* (600 nM) forward, 5'-GCG ATGTCGCACGGTACCTG-3' and reverse, 5'-GGCATG GTTACTGCCTCTGG-3'. Thermocycling conditions were as follows: Initial denaturation at 90˚C for 10 min, followed by 40 two-step PCR cycles at 95˚C for 15 sec and 60˚C for 10 sec. Results were analyzed with v2.3 StepOne® software (Thermo Fisher Scientific, Inc.), using *hprt1* (hypoxanthine phosphoribosyltransferase 1) as a endogenous control (300 nm; forward, 5'-AACGTCTTGCTCGAGATGTG-3' and reverse, 5'-GCT TTGATGTAATCCAGCAGG-3'). Quantitative determination of SA-β-gal (Senescence-associated beta-galactosidase) activity was performed using Senescence β-Galactosidase Staining kit (Cell Signaling Technology, Inc.) according to the manufacturer's instructions. Quantification was made by manually counting positive-stained cells in four randomly selected fields/well in a inverted light microscope at a magnification of 100x (Leica Microsystems). The percentage of positive cells is expressed as the mean ± SD.

Evaluation of apoptosis. Apoptosis was determined based on differential expression of apoptosis-associated *bcl2* and *bax* in treated and control MDA MB 231 cells via qPCR (ΔΔCq method) (15) using SYBR-Green (StepOne™ System; Thermo Fisher Scientific, Inc.). Primer sequences were as follows: *bcl-2* (125 nM) forward, 5'-GGATGCCTTTGTGGAACTGTAC-3'

and reverse, 5'-TTCACTTGTGGCCCAGATAGG-3' and *bax* (500 nM) forward, 5'-GGCCGGGTTGTCGCCCTTTT-3' and reverse, 5'-CCGCTCCCGGAGGAAGTCCA-3'. Thermocycling conditions were as follows: Initial denaturation at 90˚C for 10 min, followed by 40 two-step PCR cycles at 95˚C for 15 sec and 60˚C for 10 sec. Results were analyzed with v2.3 StepOne (Thermo Fisher Scientific, Inc.) software using *hprt1* as endogenous control (300 nm; forward, 5'-AACGTCTTGCTCGAGATG TG-3' and reverse, 5'-GCTTTGATGTAATCCAGCAGG-3'). MDA MB 231 apoptosis was determined via Caspase 3 activity measurement using CaspACE™ Assay System according to the manufacturer's instructions (Promega Corporation).

Generation of novel ligands and screening. With candidate R1D2-10 as the seed compound, a library of 100 novel derivatives was generated using the LigDream web server with its default parameters (16). LigDream is a machine learning-based software that uses convolutional and recurrent neural networks to generate Simplified Molecular Input Line Entry Specification (SMILES) sequences of novel compounds based on characteristics of the seed molecule (playmolecule.com/LigDream/).

SMILES sequences were converted to Protein Data Bank (PDB) format using RDKit (rdkit.org/), a specific cheminformatics Python library (17). The 3D structures of the molecules were optimized using the UFF (universal force field) (18) and converted to PDB Partial Charge & Atom Type format using the AutoDockTools software suite Version 1.5.7 (19).

Docking assay of novel ligands was performed with the same parameters in DBVS as previously described (11). The interaction between ligands and protein was analyzed using Protein-Ligand Interaction Profile (PLIP) software Version 2.2.2 (20) to identify which novel ligands bound to hDKC1 with a better docking energy than candidate R1D2-10 while also establishing strong interactions with hDKC1 key residue (plip-tool.biotec.tu-dresden.de/plip-web/plip/index).

In vitro R1D2-10 cell viability evaluation in normal primary culture derived from p4 neonatal mouse brain. Isolation and plating of mixed cortical cells were carried out following the procedure described by Schildge *et al* (21). A total of $2.5x10^4$ cells from primary culture was seeded in DMEM (Thermo Fisher Scientific, Inc.) supplemented with 10% heat-inactivated FBS (Sigma-Aldrich; Merck KGaA), 2 mM glutamine and 80 μg/ml gentamicin at 37˚C in 5% CO_2 atmosphere. Following 72 h treatment with compound R1D2-10, viable cells were determined by trypan blue 0,4% p/v staining (Thermo Fisher Scientific, Inc.) following supplier's recommendations. Then, stained cells were load in hemocytometer and manually counting (4 wells/condition) in an inverted light microscope at a magnification of 200 X (Leica Microsystems GmbH). Data were analyzed by two-way ANOVA followed by Dunnett's test and are presented as the mean ± SEM (n=3).

ADME properties, off-target interaction and toxicity prediction. Compound physicochemical and pharmacokinetic properties were analyzed using ADME descriptor algorithm (https://biosig.lab.uq.edu.au/pkcsm/prediction). The online server pkCSM ADME was used to analyze the ADME descriptors such as absorption, solubility, cytochrome CYP2D6, plasma protein binding, distribution volume (VDss), fraction unbound (human) and central nervous system (CNS) and blood-brain barrier membrane permeability (22). Off-target protein interaction was analyzed using Swiss Target Prediction tool 2019 version (23). Toxicity parameters (hepatotoxicity, skin sensitization, mutagenic and tumorigenic, reproductive toxicity, irritant) were analyzed by using DataWarrior software version 5.5.0 (24). The prediction process relies on a precomputed set of structural fragment that give rise to toxicity alerts in case they are encountered in the structure drawn. (openmolecules.org/propertyexplorer/toxicity-assessment.html).

Chemical diversity of compounds. Similarity of candidate analogs was estimated to identify chemical diversity. Molecular fingerprints encode the presence or absence of structural features in a molecule as a bit vector (25,26). Once the molecular fingerprint describing two molecules is generated, a similarity coefficient is computed. The present study used Tanimoto coefficient of similarity (27,28), which ranges from 0 to 1, where 1 implies identity. Thus, low Tanimoto coefficient of similarity implies dissimilarity.

The present study used four types of fingerprint to estimate the similarity between molecules using Tanimoto coefficient of similarity. First, 1,024-bit Morgan 2D fingerprints with a radius of 2 were calculated using RDKit (17). Furthermore, Murcko scaffold (29) of each molecule was extracted using RDKit and 1024-bit Morgan 2D fingerprint was calculated. Molecular access system (MACCS) 166 keys (30) were calculated using RDKit. MACCS keys are a coarse-grain fingerprint where each key is associated with a SMILES arbitrary target specification pattern (31). Lastly, the 1,024-bit Extended 3D fingerprints (32) were calculated for the best conformer following UFF energy minimization.

Statistical analysis. All data are presented as the mean ± SEM. Comparisons between >2 groups, the significance of differences was determined using one-way ANOVA followed by post hoc Dunnett's test. In case were analyzed only two groups were determined by unpaired T-test. The analyses were made using GraphPad Prism 6® (GraphPad Software, Inc.). $P<0.05$ was considered to indicate a statistically significant difference.

Results

R1D2-10 and R1D2-15 inhibit MDA MB 231 cell proliferation. To define concentrations for long-term treatment assay, proliferation assay was performed on MDA MB 231 cells. At low concentrations (3-25 μM) there was a cytotoxic effect in a concentration-dependent manner for both compounds (data not shown). For compound R1D2-10 and R1D2-15, IC_{50} value was 9.52 and 12.95 μM, respectively (Fig. 2). Also, maximum response (E_{max}) and goodness of fit (R^2) were calculted for both curves, obataing a E_{max}: 60.15% and R^2: 0.76 for R1D2-10 and a E_{max}: 62.71%, R^2: 0.81 for R1D2-15. Since chronic treatment requires use of the non-cytotoxic concentrations to evaluate the long-term effect of the active agents, 2 μM was selected for both compounds as this concentration was below IC_{25} and exhibited minimal cytotoxic effects.

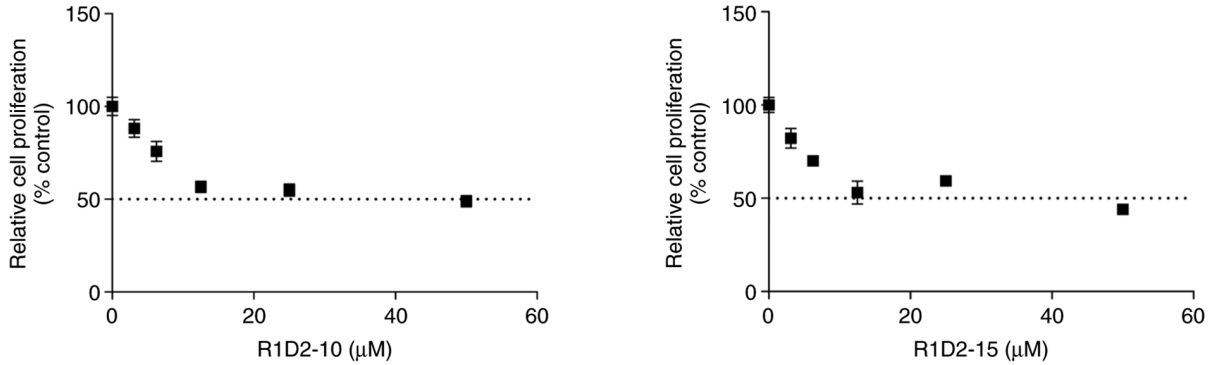

Figure 2. Effect of R1D2-10 and R1D2-15 on cell proliferation. Determination of half maximal inhibitory concentration of the compounds on MDA MB 231 cell line by MTT assay. Data are presented as the mean ± SEM (n=3).

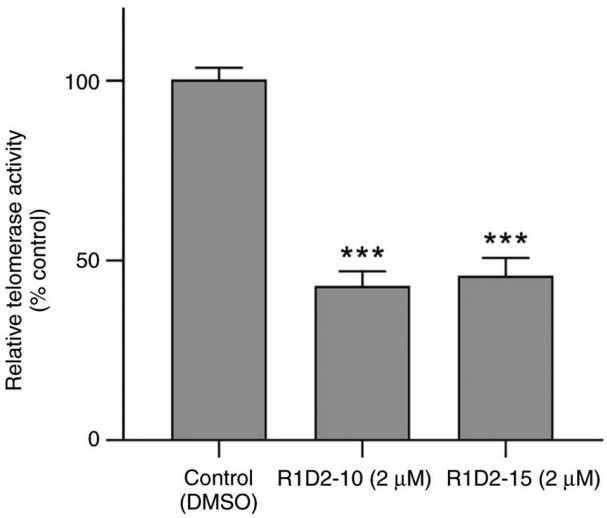

Figure 3. Determination of relative telomerase activity by real-time quantitative telomerase repeat amplification protocol. Quantification of relative telomerase activity was performed by real-time PCR with specific primers using template protein extract from treated and untreated cells for 48 h. Data were analyzed by one-way ANOVA followed by Dunnett's test and are presented as the mean ± SEM (n=6). ***P<0.001 vs. control.

R1D2-10 and R1D2-15 inhibit telomerase activity of MDA MB 231 cells. Telomerase activity was determined following 48 h treatment with potential inhibitors. R1D2-10 and R1D2-15 inhibited telomerase activity of by 57.3 and 54.6%, respectively (P<0.001; Fig. 3). Therefore 2 μM was used for chronic exposure of cells to compounds R1D2-10 and R1D2-15 to evaluate parameters as treatment progresses.

R1D2-10 and R1D2-15 chronic treatment cause telomere shortening in MDA MB 231 cell line. Telomere length following treatment was determined at 10, 25, 40 and 55 cell passages. R1D2-10 and R1D2-15 chronic exposure, exhibit a downward trend in telomere length until passage 40 (Fig. 4). There was no significant variation between passages 40 and 55 in both to R1D2-10 as R1D2-15 treated cells. Chronic treatment with R1D2-10 or R1D2-15 exhibited a decrease in telomere length of 66 and 43%, respectively, after 55 passages (P<0.001).

Considering that telomere shortening triggers senescence and apoptosis (33-35), entry into these processes was evaluated following cell treatment.

R1D2-10 treatment induces senescence in MDA MB 231 cell line. Gene expression of two senescence-associated markers was analyzed. Expression of *glb1* did not change significantly compared with the control following treatment with both compounds (Fig. 5A). Same results were obtained for *p16ink4a* expression following treatment with R1D2-15. However, after-chronic treatment with R1D2-10, expression of this marker increased more than four times in comparison with untreated cells (Fig. 5B).

Senescence-associated β galactosidase activity of treated cells was evaluated. Control and cells treated with compound R1D2-15 did not show positive staining for β galactosidase activity (Fig. 5C). However, 17.4±4.3% of R1D2-10-treated cells exhibited blue staining associated with senescence-associated β galactosidase activity (red arrows), in addition to an enlarged and rounded morphology with cytoplasmic vacuolization, consistent with senescence (black arrows; Fig. 5C).

R1D2-10 promotes apoptosis in MDA MB 231 cells. Apoptosis was evaluated by expression of anti- and pro-apoptotic *bcl2*/*bax*, and Caspase 3 activity of cells following chronic treatment with compounds R1D2-10 and R1D2-15. R1D2-10 and R1D2-15 decreased Bcl2 expression by 40 and 35%, respectively (P<0.001 and P<0.01, respectively; Fig. 6A). Regarding Bax expression, an increase of 30% was observed following treatment with R1D2-10, whereas no difference following R1D2-15 treatment was observed (Fig. 6B). Bax/Bcl2 ratio was 2.3 and 2.0 following treatment with R1D2-10 and R1D2-15, respectively (P<0.001 and P<0.01, respectively; Fig. 6C).

Caspase 3 activity was measured in treated cell lysate. Treatment with compound R1D2-10 led to a 55% increase in activity compared with control cells (P<0.01; Fig. 6D), whereas R1D2-15 exhibited similar activity to untreated cells.

Based on *in vitro* analysis of telomere length, senescence and apoptosis, R1D2-10 was selected for subsequent experiments.

R1D2-10 inhibits telomerase in other breast cancer cell lines. The aforementioned experiments were performed on MDA MB 231 cells, which correspond to a basal-claudin low breast cancer subtype. To eliminate the possibility that the inhibitory effect was cell line-dependent, the effect of R1D2-10 on IC_{50} value and telomerase activity was assessed in luminal A MCF-7 and basal MDA MB 468 cells. For MCF-7 and MDA

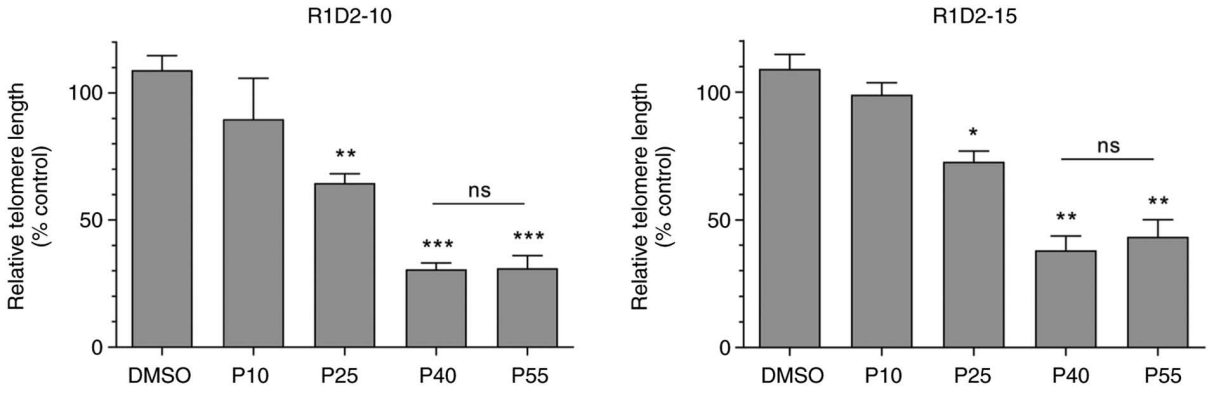

Figure 4. Determination of telomere length by quantitative PCR. Quantification of telomere length was performed by real-time PCR with specific primers using template genomic DNA from R1D2-10 and R1D2-15 treated and control (DMSO) cells at P10, 25, 40 and 55. Data were analyzed by one-way ANOVA followed by Dunnett's test and are presented as the mean ± SEM (n=3). *P<0.05, **P<0.01, ***P<0.001 vs. control (DMSO). P, passage; ns, non-significant.

MB 468, IC_{50} values were 5.95 (E_{max}: 67.56%, R^2: 0.90) and 9.79 μM (E_{max}: 73.36%, R^2: 0.91), respectively (Fig. 7A and B). Therefore, 2 μM was selected to evaluate telomerase activity. R1D2-10 treatment for 48 h caused telomerase inhibition of 64.7 in MCF-7 and 30.8% in MDA MB 468 cells (Fig. 7C and D; P<0.05). Furthermore, telomerase activity assay was assessed, to validate drug response. MDA MB 231 cells were treated with increasing concentrations of R1D2-10 for 48 h and then evaluted by RQ-TRAP. As is shown in Fig. S1, concentration-dependent behavior was observed, reaching a significant inhibition of more than 80% at the higher concentration (P<0.001).

R1D2-10 shows low cytotoxic effect on nomal culture. A lead compound that exhibits the desired biological activity and its optimization is a key step in drug discovery. Absence of toxicity against healthy cells is a sought feature. Therefore, the present study evaluated *in vitro* toxicity in a normal primary culture derived from a p4 neonatal mouse brain. The results showed no significant cytotoxic effect below 25 μM (Fig. S2). Furthermore, preliminary assays in BALB/c mice revealed no toxic effect *in vivo*. (data not shown).

R1D2-10 analogs shows improved affinity to DKC1. Considering the aforementioned results, it was hypothesized that R1D2-10 serves as a bioactive molecule *in vitro* and may be used as a seed molecule for analog design. To obtain novel candidates with improved activity, R1D2-10 analogs were generated using LigDream web server. A total of 100 candidates was obtained and used to perform docking assay using previously reported parameters (11). Fig. 8 shows docking energy value for each analog.

Analogs that exhibited greater affinity than that predicted for R1D2-10 were selected to analyze whether the novel compounds exhibited the same interactions with hDKC1 residues as R1D2-10 (hydrogen bond and π-stacking). Table I summarizes residue interactions of R1D2-10 and the selected analogs. As a result of this analysis, we selected analogs that showed improved affinity values for the target while maintaining the main interactions of R1D2-10.

R1D2-10 analogs prediction on ADME and toxicity properties. Pharmacokinetics, drug-likeness and medicinal chemistry profile of analogs were evaluated using pkCSM ADME descriptors algorithm protocol (Table II). All analogs complied with Lipinski's rule of five (data not shown). All analogs showed suitable profiles of ADME parameters. Caco-2 permeability, intestinal absorption (human) and skin permeabilization were used to predict the absorption level of compounds. When Papp coefficient is $>8x10^{-6}$, the predicted value is >0.90; thus, the compound has high Caco-2 permeability and is easy to absorb (36). R1D2-10(10, 12, 44 and 76) were predicted to have highest Caco-2 permeability, followed by R1D2-10(2, 26, 82 and 89). Intestinal absorption <30% is considered to be poorly absorbed (37). All the compounds were predicted to have absorption >88% (Table II). Logarithmic skin permeation coefficient (logKp) >-2.5 is considered to indicate relatively low skin permeability. All analyzed compounds showed logKp<2.5 and were considered to have suitable skin permeability.

Distribution volume (VDss), fraction unbound (human) and central nervous system (CNS) and blood-brain barrier membrane permeability (logBB) were evaluated to characterize the distribution of compounds. VDss describes the relationship between the concentration of drug in the plasma and the body (38). VDss<0.71 l/kg (log VDss<-0.15) is considered to be relatively low; VDss>2.81 l/kg (log VDss >0.45) is considered to be relatively high (36). VDss of R1D2-10(2, 12, 17, 24 and 79) was low, whereas compounds R1D2-10(10) and (82) showed relatively high values. For blood-brain barrier membrane permeability, logBB>0.3 indicates compounds cross the blood-brain barrier easily; logBB<0.3 indicates compounds do not easily cross the blood-brain barrier (39). All analogs show values of logBB lower than 0.3, so them were predicted to have low blood-brain barrier permeability. Regarding CNS crossing, logarithmic permeability surface-area product (logPS) was analyzed. All compounds show a logPS value among -1,366 and -2,370. Suenderhauf *et al* reported that drugs with logPS<-3 were predicted to not cross the central nervous system (CNS) (40). All compounds show a lopPS<-3, therefore, were predicted to cross the CNS.

Cytochrome P450 is a key enzyme system for drug metabolism in the liver. The primary subtypes of cytochrome P450 are CYP2D6 and CYP3A4 (41). R1D2-10(12, 21, 24, 26, 57 and 89) were not substrates for CYP2D6, whereas R1D2-10(5) was

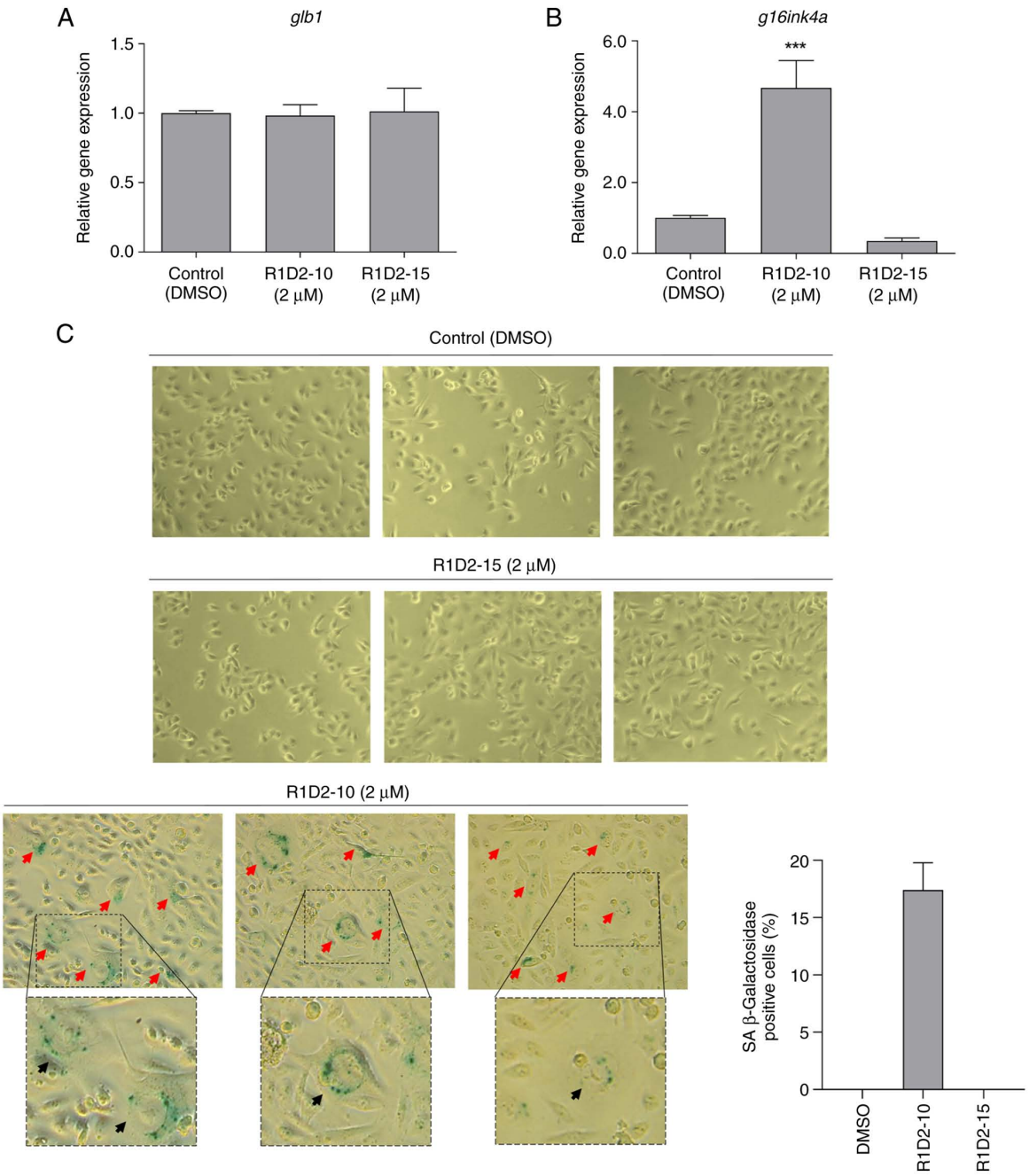

Figure 5. Evaluation of senescence after 55 passages. Relative expression of senescence-associated (A) *glb1* and (B) *p16ink4a*. Gene expression was measured by real-time PCR with specific primers using *hprt1* as endogenous control. Analysis was performed using the ΔΔCq method. Data were analyzed using one-way ANOVA followed by Dunnett's test and are presented as the mean ± SEM (n=6). ***P<0.001 vs. control (DMSO). (C) Determination of senescence-associated β-galactosidase activity by Senescence β-Galactosidase Staining kit (Magnification x100). Red arrow, positive cell; black arrow, cell with typical senescent morphology (dotted line boxes: magnification x200). Images are representative of three independent assays. *glb1*, galactosidase beta 1; *p16ink4a*, cyclin dependent kinase inhibitor 2A; *hprt1*, hypoxanthine phosphoribosyltransferase 1.

predicted to be a CYP2D6 inhibitor (Table II). By contrast, all compounds were predicted to be substrates and inhibitors of CYP3A4 (data not shown).

Drug elimination is associated with molecular weight and hydrophilicity of compounds. The prediction analysis showed that total clearance of R1D2-10(82) was highest, followed by R1D2-10(10, 12, 26 and 89). Furthermore, all candidates showed low or non-existent probability of off-target interaction (Table II).

Toxicity of compounds is shown in Table III. All the compounds were predicted to generate hepatotoxicity, except R1D2-10(10). Furthermore, R1D2-10(24, 57 and 82) exhibited high probability of generating tumorigenic effects, whereas R1D2-10(57 and 82) were also predicted to be mutagenic. Compound R1D2-10(12) was associated with reproductive toxicity.

The predicted results indicated that R1D2-10(10) was the only analog that did not show any non-desirable side effects. R1D2-10(2, 5, 17, 21, 26, 44, 76 and 89) were predicted to induce only hepatotoxicity.

Chemical diversity analysis was performed to determine whether the selected analogs were different using four molecular

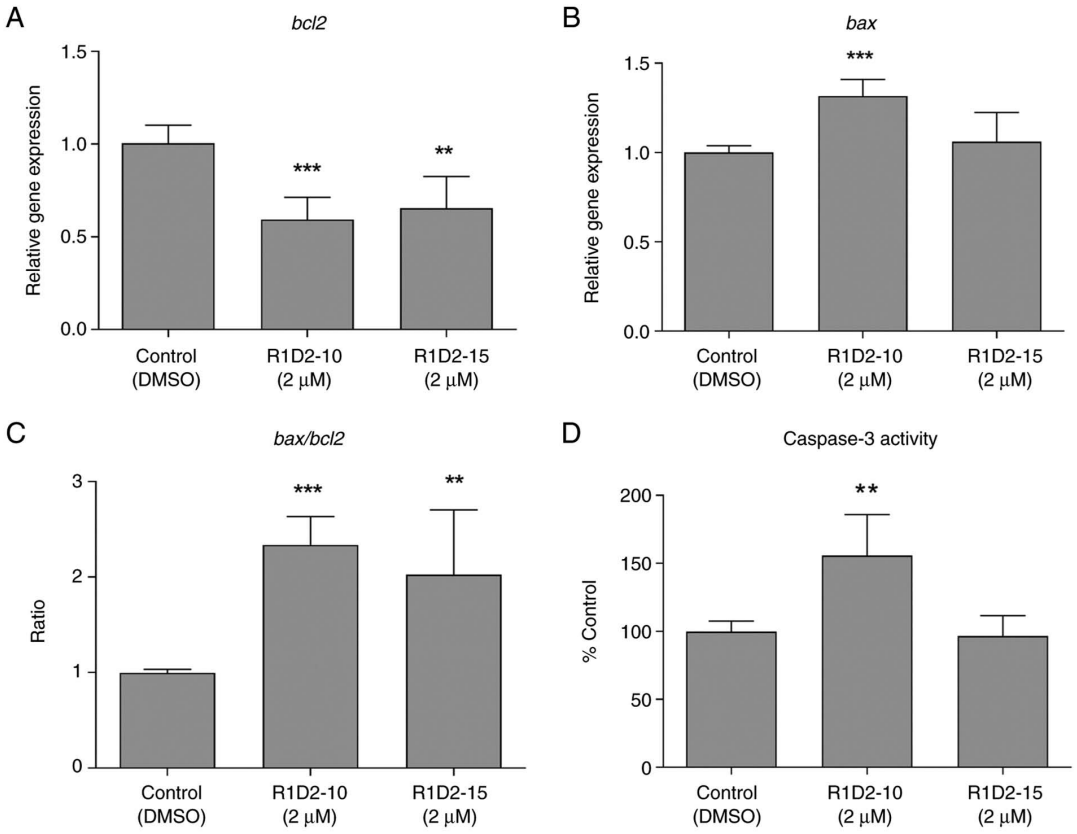

Figure 6. Effect of R1D2-10 and R1D2-15 on apoptosis. Relative expression of apoptosis-associated (A) *bcl2*, (B) *bax* and (C) *bax/bcl2* was measured by real-time PCR with specific primers, using *hprt1* as endogenous control. Analysis was performed using the ΔΔCq method. Data were analyzed using one-way ANOVA followed by Dunnett's test and are presented as the mean ± SEM (n=6). (D) Determination of Caspase 3 activity by CaspACE™ Assay System (Promega Corporation). Data were analyzed using one-way ANOVA followed by Dunnett's test and are presented as the mean ± SEM (n=3). **P<0.01, ***P<0.001 vs. control. *hprt1*, hypoxanthine phosphoribosyltransferase 1.

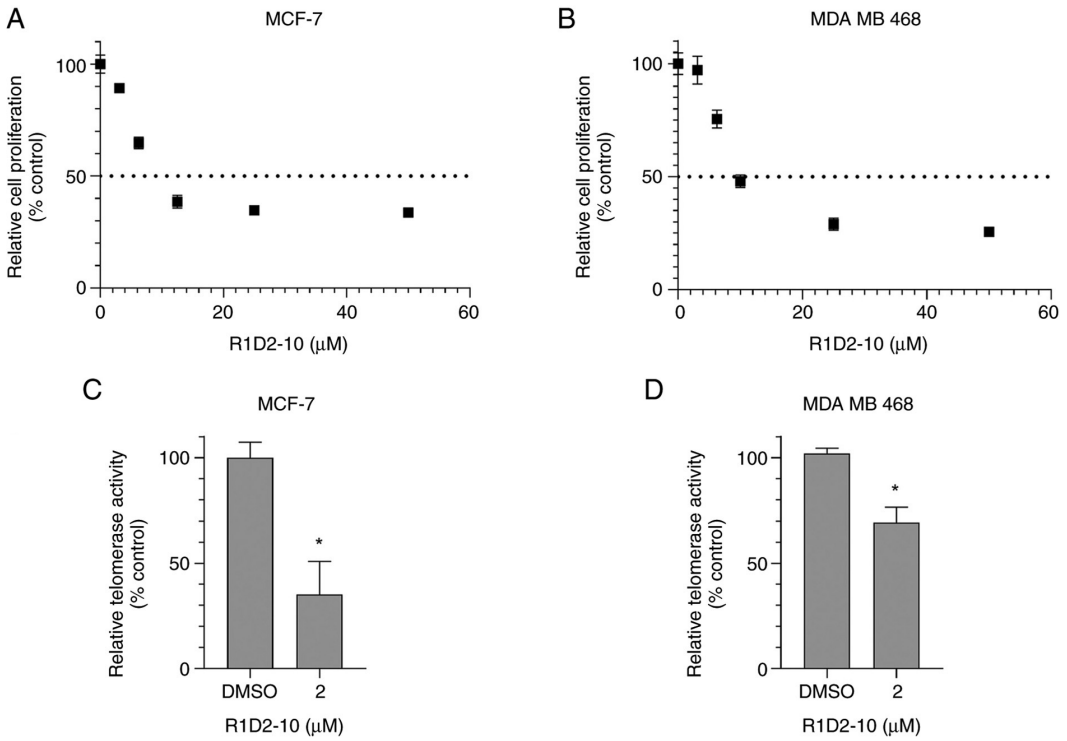

Figure 7. Effect of R1D2-10 on cell proliferation and determination of relative telomerase activity by real-time quantitative telomerase repeat amplification protocol in MCF-7 and MDA MB 468 cell lines. Determination of half maximal inhibitory concentration in (A) MCF-7 and (B) MDA MB 468 cells by MTT assay. Quantification of relative telomerase activity was performed by real-time PCR with specific primers, using template protein extract from treated and untreated (C) MCF-7 and (D) MDA MB 468 cells for 48 h. Data are presented as the mean ± SEM (n=3). *P<0.05 vs. control (Unpaired t test).

Table I. Analog interaction with specific residues of hDKC1.

Compound	Docking energy, Kcal/mol	hDKC1 residue interaction					
		Ala 305	Ala 308	Lys 314	Met 316	Gly 319	Tyr 311
R1D2-10	-6.6	H	H	2HB	HB	HB	π
R1D2-10(02)	-6.7	-	-	-	HB	HB	2H
R1D2-10(05)	-6.9	-	-	-	H	HB	H
R1D2-10(10)	-7.0	H	-	-	HB	-	π
R1D2-10(11)[a]	-6.7	H	-	-	-	-	H
R1D2-10(12)	-7.0	H	-	-	H	-	H, π
R1D2-10(17)	-6.9	H	-	-	-	-	H, π
R1D2-10(20)[a]	-7.1	H	-	-	H	-	2H
R1D2-10(21)	-7.0	H	-	-	-	-	Π
R1D2-10(24)	-7.0	-	-	H	-	-	-
R1D2-10(26)	-6.7	H	-	-	H	-	H, 2π
R1D2-10(44)	-6.9	-	-	-	H	-	Π
R1D2-10(55)[a]	-6.9	H	-	-	-	-	2H
R1D2-10(57)	-6.7	H	-	-	-	-	H, π
R1D2-10(76)	-6.9	H	-	-	-	-	Π
R1D2-10(79)[a]	-6.8	H	-	-	-	-	3H
R1D2-10(81)[a]	-6.7	H	-	-	H	-	H
R1D2-10(82)	-6.8	H	-	-	-	-	H, π
R1D2-10(89)	-7.1	H	-	-	HB	HB	2H

[a]Discarded following analysis. hDKC1, dyskerin; H, hydrophobic interaction; HB, hydrogen bond; π, π-stacking interaction; -, not applicable.

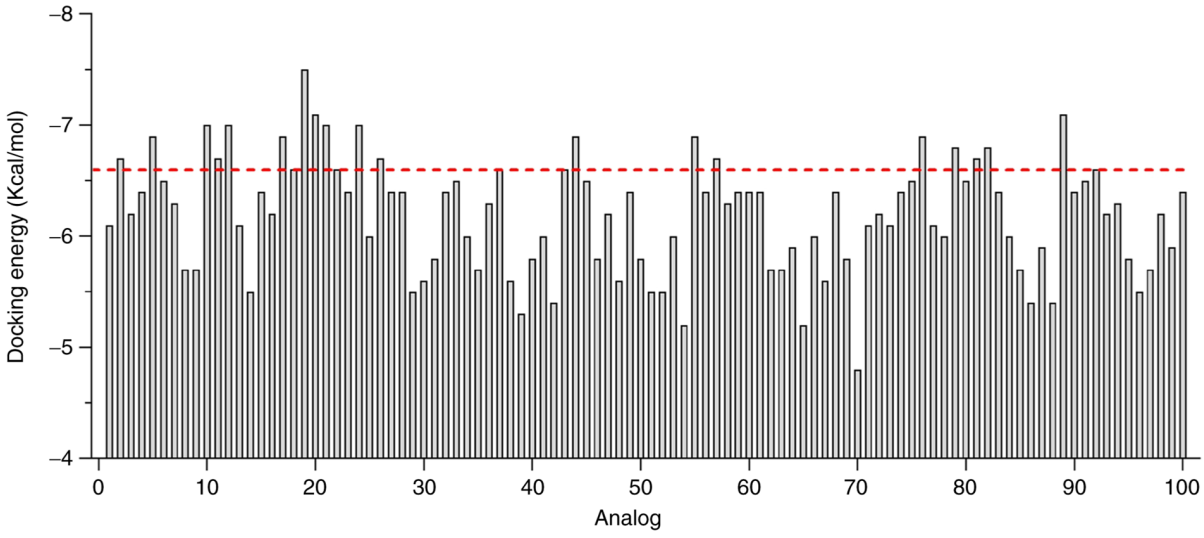

Figure 8. Docking assay of analog library. Red line indicates the docking energy of R1D2-10 (-6.6 Kcal/mol).

fingerprints and Tanimoto coefficient. MACCS fingerprint similarity values were notably higher compared with the other fingerprints (Fig. 9). Morgan 2D and Murcko Scaffold fingerprints analyze similarity based on two-dimensional molecular structure and its backbone (32,42), respectively. These results indicated no similarity among the selected compounds. Furthermore, 3D extended fingerprint analysis demonstrated lower levels of similarity than the aforementioned fingerprints. Given that low similarity values imply dissimilarity (Tanimoto coefficient <0.8) (43,44), these results indicated that the selected analogs derived from a common parent compound represent a diverse analog family and may exhibit different activity.

Discussion

The use of telomerase as an antitumor target presents various advantages. It is a key and specific component of most tumor cells and it is widely expressed in multiple types of tumor (10).

Table II. Analog ADME properties and off-target prediction. Analysis was performed using pkCSM ADMET descriptors algorithm protocol. All analogs agree with Lipinski's rules.

	Absorption						Distribution				Metabolism			Excretion		
Compound	WS, log mol/l	Caco2 P, log Papp	HIA, %	SP, log log Kp	PgP S	PgP I	VDss, log log l/kg	FU	BBB P, log BB	CNS P, log PS	CYP2D6 S	CYP2D6 I	CYP2C9 I	TC, log ml/min/kg	Renal OCT2 S	Off-target IP
R1D2-10	-3.828	0.764	91.456	-2.735	Yes	Yes	-0.385	0.011	0.051	-1.564	Yes	No	Yes	0.554	No	Low
R1D2-10(02)	-4.363	0.827	88.163	-2.735	Yes	Yes	-0.601	0.013	-0.757	-1.468	Yes	No	Yes	0.239	No	Low
R1D2-10(05)	-3.863	0.707	88.938	-2.769	Yes	Yes	0.044	0.117	-0.553	-1.922	Yes	Yes	Yes	0.301	No	Low
R1D2-10(10)	-3.693	1.011	92.107	-2.745	Yes	Yes	0.672	0.019	-0.849	-1.967	Yes	No	Yes	0.452	No	Low
R1D2-10(12)	-4.374	1.032	92.389	-2.735	Yes	Yes	-0.494	0.015	-0.518	-2.181	No	No	Yes	0.476	No	NE
R1D2-10(17)	-4.152	0.732	89.153	-2.736	Yes	Yes	-0.400	0.000	-0.569	-1.749	Yes	No	Yes	0.308	No	NE
R1D2-10(21)	-4.391	0.556	94.679	-2.759	Yes	Yes	-0.080	0.027	-0.867	-1.964	No	No	Yes	0.359	No	Low
R1D2-10(24)	-5.371	0.609	95.679	-2.735	Yes	Yes	-1.083	0.088	0.081	-1.366	No	No	Yes	0.240	No	Low
R1D2-10(26)	-3.587	0.893	94.051	-2.735	Yes	Yes	-0.023	0.000	-0.776	-1.869	No	No	Yes	0.489	No	NE
R1D2-10(44)	-4.059	0.917	90.807	-2.870	Yes	Yes	0.414	0.086	0.034	-1.707	Yes	No	Yes	0.358	No	Low
R1D2-10(57)	-5.097	0.539	93.358	-2.753	Yes	Yes	-0.272	0.000	-0.054	-1.748	No	No	Yes	0.284	No	Low
R1D2-10(76)	-4.058	1.053	91.659	-2.843	Yes	No	-0.106	0.050	-1.084	-1.991	Yes	No	Yes	0.294	No	Low
R1D2-10(82)	-4.082	0.892	92.963	-2.742	Yes	Yes	0.740	0.052	0.199	-1.957	Yes	No	Yes	1.090	No	Low
R1D2-10(89)	-4.098	0.892	93.241	-2.763	Yes	No	0.108	0.048	-0.762	-2.370	No	No	No	0.437	No	Low

WS, water solubility; P, permeability; HIA, human intestinal absorption; SP, skin permeabilization; Kp, skin permeation coefficient; Pgp, P-glycoprotein; VDss, volume of distribution; FU, fraction unbound; BBB, blood-brain barrier; BB, Brain Blood; CNS, central nervous system; PS, permeability surface; I, inhibitor; TC, total clearance; OCT2, Organic Cation Transporter 2; S, substrate; IP, interaction probability; NE, no effect predicted.

Table III. Prediction of analog toxicity. Analysis was performed using DataWarrior software (24).

Compound	Hepatotoxicity	Skin sensitization	Mutagenic	Tumorigenic	Reproductive toxicity	Irritant
R1D2-10	Yes[a]	No	None	None	None	None
R1D2-10(02)	Yes[a]	No	None	None	None	None
R1D2-10(05)	Yes[a]	No	None	None	None	None
R1D2-10(10)	No	No	None	None	None	None
R1D2-10(12)	Yes[a]	No	None	None	Low[b]	None
R1D2-10(17)	Yes[a]	No	None	None	None	None
R1D2-10(21)	Yes[a]	No	None	None	None	None
R1D2-10(24)	Yes[a]	No	None	High[a]	None	None
R1D2-10(26)	Yes[a]	No	None	None	None	None
R1D2-10(44)	Yes[a]	No	None	None	None	None
R1D2-10(57)	Yes[a]	No	High[a]	High[a]	None	None
R1D2-10(76)	Yes[a]	No	None	None	None	None
R1D2-10(82)	Yes[a]	No	High[a]	High[a]	None	None
R1D2-10(89)	Yes[a]	No	None	None	None	None

[a]High probability; [b]low probability.

Moreover, telomerase is the most common mechanism to evade replicative mortality by tumoral cells. Only one less robust compensatory process exists: Alternative lengthening of telomeres. This may limit risk of developing resistance to telomerase inhibition-based therapy (45). On the other hand, low or null expression of telomerase in normal tissue promotes specificity and diminishes risk of toxicity in healthy cells, concluding in a promising therapeutic window (46). Telomerase inhibitors include natural compounds, immunotherapies, oligonucleotides, gene therapy, small molecules, and nucleoside analogs (8).

R1D2-10 and R1D2-15 cytotoxic effect and telomerase inhibitory capacity were evaluated on MDA MB 231 cells at 0-50 μM. Following 72 h incubation, IC_{50} values of 9.52 and 12.95 μM were obtained for R1D2-10 and R1D2-15, respectively. These results agree with those reported for other telomerase inhibitors (47-49). Furthermore, both compounds demonstrated an inhibitory effect on telomerase activity, inducing inhibition >50% following 48 h treatment. R1D2-10 showed a concentration-dependent behavior, validating the observed drug response. This effect has been reported for other telomerase inhibitors, supporting the present results (50,51).

Furthermore, in comparison with the reported effect of other telomerase inhibitors, such as Pterostilbene, BIBR1532 and AZT, R1D2-10 and R1D2-15 exhibited a greater inhibitory effect at shorter time and lower concentrations (52-54). Obtaining the desired effect using the lowest possible dose minimizes undesirable side effects. The present study aimed to evaluate capacity to inhibit telomerase activity and effect on the proliferative capacity of cells. To evaluate whether R1D2-10 and R1D2-15 lead to telomere shortening, senescence and apoptosis, cells were treated for 55 passages (~22 weeks). Considering that the aforementioned process depends on cell division, chronic telomerase inhibitor treatment is usually among this amount of cell passages (52-56).

To evaluate telomere length, a relative telomere length determination assay based on qPCR was performed. Telomere length decreased to 66 and 43% decrease for compounds R1D2-10 and R1-D2-15, respectively, after 55 passages. Similar results have been reported for chronic treatment with Imetelstat (57), MST312 (58) and BIBR1532 (59). Cell senescence is primarily caused by telomere shortening (49). Senescence involves changes in replicative capacity, cellular morphology, gene expression and metabolism (60). Senescence is commonly evaluated by SA-β galactosidase activity due to easy detection at pH 6 with artificial substrate X-gal (61) and expression of tumor suppressor gene *p16ink4a*. This gene encodes a protein that exhibits tumor suppressor functions by inhibiting CDK4 and CDK6, and then regulates cell cycle and senescence (62). The present study demonstrated a positive staining for SA-β galactosidase activity and a 4-fold increase in expression for *p16ink4a* following treatment with compound R1D2-10. Moreover, positive cells were bigger and rounded with cytoplasmic vacuolization. These results indicated that R1D2-10 treatment led to senescence entrance triggered by telomere shortening; this was comparable with the effect of other reported telomerase inhibitors (59-65). Although it has been reported that increased *glb1* expression is associated with the senescent phenotype, treatment with R1D2-10 and R1D2-15 did not affect this marker. However, we consider that this result does not invalidate our conclusion, since the positive activity observed by X-gal staining is more relevant to the senescent phenotype than a direct correlation with *glb1* mRNA levels (66).

Telomere shortening triggers both senescence and programmed cell death (34). Bcl2 protein family (Bax, Bak, Bcl2, Bcl-xL) and the effector Caspases 3 and 6 are key in regulation of apoptosis (67). Considering telomere shortening was caused by R1D2-10 and R1D2-15 treatment, the effect on *bcl2*/*bax* expression and Caspase 3 activity was evaluated. R1D2-10 generated a decrease of 40% in expression of anti-apoptotic *bcl2* and increase of 30% of pro-apoptotic *bax*. The ratio of *bax*/*bcl2* was 2.3, indicating a pro-apoptotic state compared with the control. In addition, >50% increase

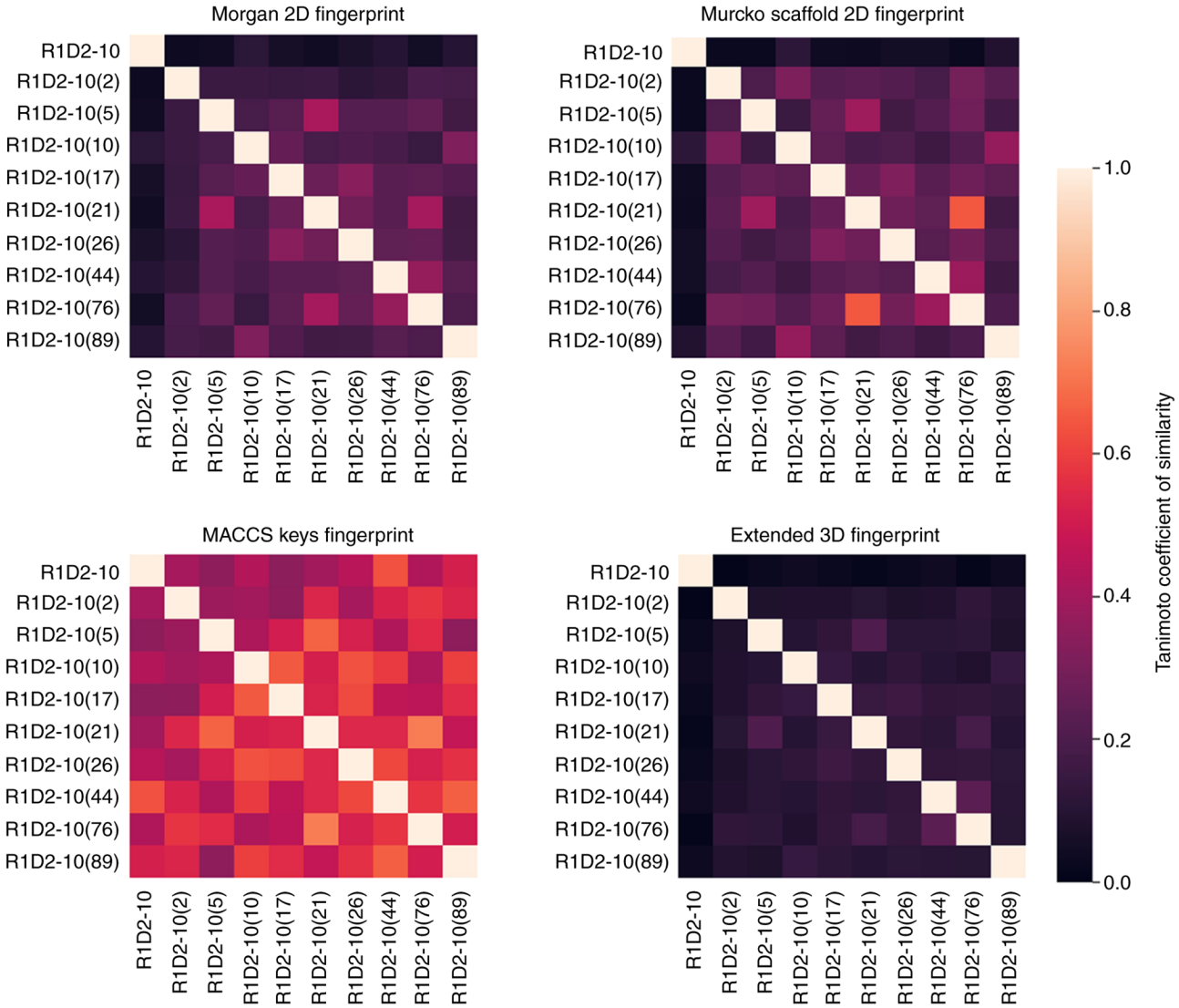

Figure 9. Chemical diversity of analogs. Estimated similarity between molecules using four types of fingerprints with Tanimoto coefficient (1 represents identity). MACCS, molecular access system.

in Caspase 3 activity was observed following treatment with R1D2-10, indicating apoptosis. These results are consistent with the pro-apoptotic effect of other telomerase inhibitors in cancer (49,65,68,69), supporting the potential role of R1D2-10 as a telomerase inhibitor with an *in vitro* antitumor effect.

By contrast with R1D2-10, cells treated with R1D2-15 showed no difference in senescence or apoptosis. Although both compounds were identified by DBVS and used at the same concentration, they have different chemical structures and different effectiveness as telomerase inhibitor and on telomere shortening. Therefore, the effect of R1D2-15 may not be enough to trigger senescence and apoptosis.

Once R1D2-10 was selected as our lead compound, we evaluate that inhibitory effect of telomerase is not dependent of the cell line. R1D2-10 inhibited telomerase activity both in MDA MB 468 and MCF-7 breast cancer cell lines, demonstrating that it could be used in different subtypes of human breast cancer.

In drug discovery, a primary feature to select a seed compound is absent or low toxicity against normal cells. As an *in vitro* toxicity assay, evaluation in primary cell culture is a relatively simple method (70). The effect of R1D2-10 was evaluated in primary cell culture from mouse brain; there was no significant cytotoxic effect <25 μM. This was considerably higher than the concentration used define for long-term treatment (2 μM). Additionally, preliminary data from *in vivo* toxicity study how no toxic effect on mice. Therefore, it was hypothesized that R1D2-10 used in our defined concentration of 2 μM had a low or null cytotoxic effect on normal cells.

After identifying a bioactive compound, the design of novel chemical entities based on the hit structure is the following step in drug discovery. Analogs based on R1D2-10 were designed using LigDream web server. This strategy is widely reported in novel drug design (71,72).

A total of 100 novel analogs was evaluated by docking assay using the same parameters as previously described (11). Considering the structural information obtained from the initial DBVS, protein-ligand interactions were used as criteria for selecting novel ligands with improved affinity compared with R1D2-10. We selected candidates that presented, preferably, hydrogen bond and π stacking interactions with the residues of

DKC1, considering that they are stronger than hydrophobic interactions (73). The selected interaction are reported to improve the affinity and selectivity of the drug with a binding site (74).

As ADME and toxicity prediction serve an important role in facilitating appropriate selection of candidate drugs by pharmaceutical companies prior to expensive clinical trials, the ADME and toxicity parameters of novel candidates were predicted (75). All analogs complied with Lipinski's rule of five, which indicates a good druggability profile, and most showed suitable values of ADME properties using the pkCSM prediction tool, which is broadly reported (22,76-78). Additionally, target prediction of small bioactive molecules was analyzed using Swiss Target Prediction (63,79). Small molecules are designed to bind to proteins or other macro-molecular targets to modulate their activity, resulting in phenotypic effects. For this reason, mapping the targets of small bioactive molecules is a key step for unraveling the molecular mechanisms underlying bioactivity and predicting potential side effects or cross-reactivity (80). All candidates were predicted to exhibit low or null probability of off-target interaction. Toxicity parameters of the analogs were assessed by DataWarrior (24,81-83); analogs that were predicted to exhibit mutagenic, tumorigenic or reproductive toxicity were discarded. A total of nine analogs with suitable parameters regarding target affinity, ADME properties, off-target interaction and undesirable side effects was obtained. Considering that we want to synthesize these candidates in order to find one with improved *in vitro* and *in vivo* effectiveness, we decided to analyze their similarity. The fundamental principle behind similarity-based study is the 'chemical similarity principle,' which states that if two molecules share similar structures, then they will likely have similar bioactivities (84) In this way, we would select the analogs that are chemically different in order to obtain different effectiveness. Several studies proposed that calculation of molecular similarity could be carried out by using small-molecule fingerprints, and these fingerprints are calculated by numerous approaches (85,86). The present study calculated four types of fingerprints with Tanimoto coefficient. These strategies are widely reported as methods of refinement and molecule characterization (87-90). Particularly, MACCS fingerprint similarity values were notably higher compared with the other fingerprints. This fact was expectable considering that MACCS fingerprint bases analysis on searching common structural patterns in drug molecules. Considering that we designed analogs from a seed molecule with drug-like features, this result supports the idea that all the selected analogs maintain these features. In Summary, analogs exhibited chemical diversity, so may exhibit different *in vitro* or *in vivo* activity. Based on the aforementioned results, we propose analogs R1D2-10(2), (5), (10), (17), (21), (26), (44), (76) and (89) as candidates to be synthesized and evaluated in further works.

The present study evaluated potential telomerase inhibitors. The jump from *in silico* to *in vitro* assay constitutes one of the most important steps of the rational design of novel drugs. Furthermore, the finding of the desired activity establishes the validation basis of the rational and experimental design.

The primary goal of antitumor telomerase-based therapy is to selectively induce cell death in tumor cells targeting unlimited replicative capacity, which is associated with apoptosis evasion.

The present *in vitro* evaluation of drug-like candidates on MDA MB 231 cells showed that R1D2-10 inhibited telomerase activity at a dose similar to that of other reported telomerase inhibitors such as BIBR1532, MST312 and Imetelstat (47,49,55); this induced telomere shortening, senescence and apoptosis.

To the best of our knowledge, destabilization of the interaction of hTR/hDKC1 complex has not been reported as a strategy for telomerase inhibition. The present results may allow development of a directed therapy based on telomerase and contributes to rational design of novel antitumor drugs.

The present study identified the hit R1D2-10, which showed activity as telomerase inhibitor and induced cell senescence and apoptosis. From this seed compound, analogs were generated to identify those with the best profile to be synthesized and evaluated. A total of nine chemically diverse analogs with suitable parameters regarding predicted affinity, ADME properties, off-target interaction and undesirable side effects was identified. These results provide a basis for preclinical assays to characterize R1D2-10 and selected analog effectiveness as antitumor therapy in breast cancer models to demonstrate their potential use in the clinic.

Acknowledgements

The authors would like to thank Dr.Andrii Buvailo from Enamine for support in the development and sinthesys of analogues. Primary mouse culture was were kindly provided by Chronobiology Laboratory (National Quilmes University, Buenos Aires, Argentina).

Funding

The present study was supported by grants from Quilmes National University (PUNQ EXPTE 1297/19), National Research Council (PIP EXPTE N° 1811/19), the National Agency for the Promotion of Science and Technology (PICT 2018 N° 2377; PICT START UP 2020 N° 00001) and Cancer National Institute (EXPTE 827-1533/18) (Argentina).

Availability of data and materials

The data generated in the present study are not publicly available due to reasons of protection of intellectual property but are available from the corresponding author on reasonable request.

Authors' contributions

RA, RV, CP, JM and DMG designed and performed *in vitro* experiments and wrote the manuscript. MC, PC and PLM contributed to R1D2-10 analog generation and *in silico* analysis and prediction. DG conceived the study. All authors have read and approved the final manuscript. RA and DG confirm the authenticity of all the raw data.

Ethics approval and consent to participate

Not applicable.

Patient consent for publication

Not applicable.

Competing interests

The authors declare that they have no competing interests.

References

1. Jafri MA, Ansari SA, Alqahtani MH and Shay JW: Roles of telomeres and telomerase in cancer, and advances in telomerase-targeted therapies. Genome Med 8: 69, 2016.
2. Berardinelli F, Coluzzi E, Sgura A and Antoccia A: Targeting telomerase and telomeres to enhance ionizing radiation effects in in vitro and in vivo cancer models. Mutat Res Rev Mutat Res 773: 204-219, 2017.
3. Lipinska N, Romaniuk A, Paszel-Jaworska A, Toton E, Kopczynski P and Rubis B: Telomerase and drug resistance in cancer. Cell Mol Life Sci 74: 4121-4132, 2017.
4. Mender I, LaRanger R, Luitel K, Peyton M, Girard L, Lai TP, Batten K, Cornelius C, Dalvi MP, Ramirez M, *et al*: Telomerase-Mediated strategy for overcoming non-small cell lung cancer targeted therapy and chemotherapy resistance. Neoplasia 20: 826-837, 2018.
5. Sengupta S, Sobo M, Lee K, Senthil Kumar S, White AR, Mender I, Fuller C, Chow LML, Fouladi M, Shay JW and Drissi R: Induced telomere damage to treat telomerase expressing therapy-resistant pediatric brain tumors. Mol Cancer Ther 17: 1504-1514, 2018.
6. Zhang G, Wu LW, Mender I, Barzily-Rokni M, Hammond MR, Ope O, Cheng C, Vasilopoulos T, Randell S, Sadek N, *et al*: Induction of telomere dysfunction prolongs disease control of therapy-resistant melanoma. Clin Cancer Res 24: 4771-4784, 2018.
7. Wu Y, Zhong D, Li Y, Wu H, Xu X, Yang J and Gu Z: Tumor-Oriented telomerase-terminated nanoplatform as versatile strategy for multidrug resistance reversal in cancer treatment. Adv Healthc Mater 9: e1901739, 2020.
8. Gomez DL, Armando RG, Cerrudo CS, Ghiringhelli PD and Gomez DE: Telomerase as a cancer target. Development of new molecules. Curr Top Med Chem 16: 2432-2440, 2016.
9. Guterres AN and Villanueva J: Targeting telomerase for cancer therapy. Oncogene 39: 5811-5824, 2020.
10. Jager K and Walter M: Therapeutic Targeting of Telomerase. Genes 7: 2016.
11. Armando RG, Mengual Gomez DL, Juritz EI, Lorenzano Menna P and Gomez DE: Homology model and docking-based virtual screening for ligands of human dyskerin as new inhibitors of telomerase for cancer treatment. Int J Mol Sci 19: 3216, 2018.
12. Jaiswal RK and Yadava PK: Assessment of telomerase as drug target in breast cancer. J Biosci 45: 72, 2020.
13. Holliday DL and Speirs V: Choosing the right cell line for breast cancer research. Breast Cancer Res 13: 215, 2011.
14. Cawthon RM: Telomere measurement by quantitative PCR. Nucleic Acids Res 30: e47, 2002.
15. Livak KJ and Schmittgen TD: Analysis of relative gene expression data using real-time quantitative PCR and the 2(-Delta Delta C(T)) Method. Methods 25: 402-408, 2001.
16. Skalic M, Jimenez J, Sabbadin D and De Fabritiis G: Shape-Based generative modeling for de novo drug design. J Chem Inf Model 59: 1205-1214, 2019.
17. RDKit: Open-source cheminformatics. GitHub and SourceForge, 2021. https://www.rdkit.org/.
18. Rappé AK, Casewit CJ, Colwell K, Goddard WA III and Skiff WM: UFF, a full periodic table force field for molecular mechanics and molecular dynamics simulations. J Am Chem Soc 114: 10024-10035, 1992.
19. Morris GM, Huey R, Lindstrom W, Sanner MF, Belew RK, Goodsell DS and Olson AJ: AutoDock4 and AutoDockTools4: Automated docking with selective receptor flexibility. J Comput Chem 30: 2785-2791, 2009.
20. Salentin S, Schreiber S, Haupt VJ, Adasme MF and Schroeder M: PLIP: Fully automated protein-ligand interaction profiler. Nucleic Acids Res 43(W1): W443-447, 2015.
21. Schildge S, Bohrer C, Beck K and Schachtrup C: Isolation and culture of mouse cortical astrocytes. J Vis Exp (71): 50079, 2013.
22. Pires DE, Blundell TL and Ascher DB: pkCSM: Predicting small-molecule pharmacokinetic and toxicity properties using graph-based signatures. J Med Chem 58: 4066-4072, 2015.
23. Daina A, Michielin O and Zoete V: SwissTargetPrediction: Updated data and new features for efficient prediction of protein targets of small molecules. Nucleic Acids Res 47(W1): W357-W364, 2019.
24. Sander T, Freyss J, von Korff M and Rufener C: DataWarrior: An open-source program for chemistry aware data visualization and analysis. J Chem Inf Model 55: 460-473, 2015.
25. Gasteiger J and Engel T: Chemoinformatics: a textbook. John Wiley & Sons, 2006. Chapter 2.9. Volume 1: 92-110, 2006.
26. Leach AR and Gillet VJ: An introduction to chemoinformatics. Springer, 2007. Chapter 5 - Similiraty Methods. Volume 1: 99-117, 2007.
27. Sharma A and Lal SP: Tanimoto based similarity measure for intrusion detection system. J Inf Sec 2: 195-201, 2011.
28. Willett P, Barnard JM and Downs GM: Chemical similarity searching. J Chem Inf Comput Sci 38: 983-996, 1998.
29. Bemis GW and Murcko MA: The properties of known drugs. 1. Molecular frameworks. J Med Chem 39: 2887-2893, 1996.
30. Durant JL, Leland BA, Henry DR and Nourse JG: Reoptimization of MDL keys for use in drug discovery. J Chem Inf Comput Sci 42: 1273-1280, 2002.
31. BIOVIA: The keys to understanding MDL keyset technology. Dassault Systemes, Waltham, MA, 2011. https://docplayer.net/64556108-The-keys-to-understanding-mdl-keyset-technology-white-paper.html
32. Axen SD, Huang XP, Caceres EL, Gendelev L, Roth BL and Keiser MJ: A Simple Representation of three-dimensional molecular structure. J Med Chem 60: 7393-7409, 2017.
33. Deng Y, Chan SS and Chang S: Telomere dysfunction and tumour suppression: The senescence connection. Nat Rev Cancer 8: 450-458, 2008.
34. Roake CM and Artandi SE: Control of cellular aging, tissue function, and cancer by p53 downstream of telomeres. Cold Spring Harb Perspect Med 7: a026088, 2017.
35. Lin J and Epel E: Stress and telomere shortening: Insights from cellular mechanisms. Ageing Res Rev 73: 101507, 2022.
36. Han Y, Zhang J, Hu CQ, Zhang X, Ma B and Zhang P: In silico ADME and toxicity prediction of ceftazidime and its impurities. Front Pharmacol 10: 434, 2019.
37. Hou T, Wang J, Zhang W and Xu X: ADME evaluation in drug discovery. 7. Prediction of oral absorption by correlation and classification. J Chem Inf Model 47: 208-218, 2007.
38. Holt K, Nagar S and Korzekwa K: Methods to predict volume of distribution. Curr Pharmacol Rep 5: 391-399, 2019.
39. Muehlbacher M, Spitzer GM, Liedl KR and Kornhuber J: Qualitative prediction of blood-brain barrier permeability on a large and refined dataset. J Comput Aided Mol Des 25: 1095-1106, 2011.
40. Suenderhauf C, Hammann F and Huwyler J: Computational prediction of blood-brain barrier permeability using decision tree induction. Molecules 17: 10429-10445, 2012.
41. McDonnell AM and Dang CH: Basic review of the cytochrome p450 system. J Adv Pract Oncol 4: 263-268, 2013.
42. Laufkotter O, Sturm N, Bajorath J, Chen H and Engkvist O: Combining structural and bioactivity-based fingerprints improves prediction performance and scaffold hopping capability. J Cheminform 11: 54, 2019.
43. Bajusz D, Racz A and Heberger K: Why is Tanimoto index an appropriate choice for fingerprint-based similarity calculations? J Cheminform 7: 20, 2015.
44. Snarey M, Terrett NK, Willett P and Wilton DJ: Comparison of algorithms for dissimilarity-based compound selection. J Mol Graph Model 15: 372-385, 1997.
45. Zhang JM and Zou L: Alternative lengthening of telomeres: From molecular mechanisms to therapeutic outlooks. Cell Biosci 10: 30, 2020.
46. Shay JW and Wright WE: Telomeres and telomerase in normal and cancer stem cells. FEBS Lett 584: 3819-3825, 2010.
47. Gurung RL, Lim SN, Low GK and Hande MP: MST-312 alters telomere dynamics, gene expression profiles and growth in human breast cancer cells. J Nutrigenet Nutrigenomics 7: 283-298, 2014.
48. Kazemi-Lomedasht F, Rami A and Zarghami N: Comparison of inhibitory effect of curcumin nanoparticles and free curcumin in human telomerase reverse transcriptase gene expression in breast cancer. Adv Pharm Bull 3: 127-130, 2013.
49. Wardi L, Alaaeddine N, Raad I, Sarkis R, Serhal R, Khalil C and Hilal G: Glucose restriction decreases telomerase activity and enhances its inhibitor response on breast cancer cells: Possible extra-telomerase role of BIBR 1532. Cancer Cell Int 14: 60, 2014.
50. Noureini SK and Wink M: Dose-dependent cytotoxic effects of boldine in HepG-2 cells-telomerase inhibition and apoptosis induction. Molecules 20: 3730-3743, 2015.

51. Yang YL, Huang PH, Chiu HC, Kulp SK, Chen CS, Kuo CJ, Chen HD and Chen CS: Histone deacetylase inhibitor AR42 regulates telomerase activity in human glioma cells via an Akt-dependent mechanism. Biochem Biophys Res Commun 435: 107-112, 2013.
52. Bashash D, Ghaffari SH, Mirzaee R, Alimoghaddam K and Ghavamzadeh A: Telomerase inhibition by non-nucleosidic compound BIBR1532 causes rapid cell death in pre-B acute lymphoblastic leukemia cells. Leuk Lymphoma 54: 561-568, 2013.
53. Chen RJ, Wu PH, Ho CT, Way TD, Pan MH, Chen HM, Ho YS and Wang YJ: P53-dependent downregulation of hTERT protein expression and telomerase activity induces senescence in lung cancer cells as a result of pterostilbene treatment. Cell Death Dis 8: e2985, 2017.
54. Fang JL and Beland FA: Long-term exposure to zidovudine delays cell cycle progression, induces apoptosis, and decreases telomerase activity in human hepatocytes. Toxicol Sci 111: 120-130, 2009.
55. Hu Y, Bobb D, He J, Hill DA and Dome JS: The HSP90 inhibitor alvespimycin enhances the potency of telomerase inhibition by imetelstat in human osteosarcoma. Cancer Biol Ther 16: 949-957, 2015.
56. Tejera AM, Alonso DF, Gomez DE and Olivero OA: Chronic in vitro exposure to 3'-azido-2', 3'-dideoxythymidine induces senescence and apoptosis and reduces tumorigenicity of metastatic mouse mammary tumor cells. Breast Cancer Res Treat 65: 93-99, 2001.
57. Frink RE, Peyton M, Schiller JH, Gazdar AF, Shay JW and Minna JD: Telomerase inhibitor imetelstat has preclinical activity across the spectrum of non-small cell lung cancer oncogenotypes in a telomere length dependent manner. Oncotarget 7: 31639-31651, 2016.
58. Morais KS, Guimaraesb AFR, Ramos DAR, Silva FP and de Oliveira DM: Long-term exposure to MST-312 leads to telomerase reverse transcriptase overexpression in MCF-7 breast cancer cells. Anticancer Drugs 28: 750-756, 2017.
59. Mueller S, Hartmann U, Mayer F, Balabanov S, Hartmann JT, Brummendorf TH and Bokemeyer C: Targeting telomerase activity by BIBR1532 as a therapeutic approach in germ cell tumors. Invest New Drugs 25: 519-524, 2007.
60. van Deursen JM: The role of senescent cells in ageing. Nature 509: 439-446, 2014.
61. Sharpless NE and Sherr CJ: Forging a signature of in vivo senescence. Nat Rev Cancer.15: 397-408, 2015.
62. Zhao R, Choi BY, Lee MH, Bode AM and Dong Z: Implications of genetic and epigenetic alterations of CDKN2A (p16(INK4a)) in cancer. EBioMedicine 8: 30-39, 2016.
63. Liang Y, Liang B, Wu XR, Chen W and Zhao LZ: Network pharmacology-based systematic analysis of molecular mechanisms of dingji fumai decoction for ventricular arrhythmia. Evid Based Complement Alternat Med 2021: 5535480, 2021.
64. Bernadotte A, Mikhelson VM and Spivak IM: Markers of cellular senescence. Telomere shortening as a marker of cellular senescence. Aging (Albany NY) 8: 3-11, 2016.
65. Burchett KM, Yan Y and Ouellette MM: Telomerase inhibitor imetelstat (GRN163L) limits the lifespan of human pancreatic cancer cells. PloS One 9: e85155, 2014.
66. Lee BY, Han JA, Im JS, Morrone A, Johung K, Goodwin EC, Kleijer WJ, DiMaio D and Hwang ES: Senescence-associated beta-galactosidase is lysosomal beta-galactosidase. Aging Cell 5: 187-195, 2006.
67. Su Z, Yang Z, Xu Y, Chen Y and Yu Q: Apoptosis, autophagy, necroptosis, and cancer metastasis. Mol Cancer 14: 48, 2015.
68. Asghari-Kia L, Bashash D, Safaroghli-Azar A, Momeny M, Hamidpour M and Ghaffari SH: Targeting human telomerase RNA component using antisense oligonucleotide induces rapid cell death and increases ATO-induced apoptosis in APL cells. Eur J Pharmacol 809: 215-223, 2017.
69. Bashash D, Ghaffari SH, Zaker F, Kazerani M, Hezave K, Hassani S, Rostami M, Alimoghaddam K and Ghavamzadeh A: BIBR 1532 increases arsenic trioxide-mediated apoptosis in acute promyelocytic leukemia cells: Therapeutic potential for APL. Anticancer Agents Med Chem 13: 1115-1125, 2013.
70. Vairano M, Graziani G, Tentori L, Tringali G, Navarra P and Dello Russo C: Primary cultures of microglial cells for testing toxicity of anticancer drugs. Toxicol Lett 148: 91-94, 2004.
71. Cardama GA, Comin MJ, Hornos L, Gonzalez N, Defelipe L, Turjanski AG, Alonso DF, Gomez DE and Menna PL: Preclinical development of novel Rac1-GEF signaling inhibitors using a rational design approach in highly aggressive breast cancer cell lines. Anticancer Agents Med Chem 14: 840-851, 2014.
72. Ramana M, Lokhande R, Bhar S, Ranade P, Mehta A and Gadre G: In Silico design, synthesis and bioactivity of N-(2, 4-Dinitrophenyl)-3-oxo-3-phenyl-N-(aryl) phenyl propanamide derivatives as breast cancer inhibitors. Curr Comput Aided Drug Des 13: 112-126, 2017.
73. Gerbelli BB, Vassiliades SV, Rojas JEU, Pelin JNBD, Mancini RSN, Pereira WSG, Aguilar AM, Venanzi M, Cavalieri F, Giuntini F and Alves WA: Hierarchical Self-assembly of peptides and its applications in bionanotechnology. Bioin Bioba Mater 220: 1900085, 2019.
74. Smith AJ, Zhang X, Leach AG and Houk KN: Beyond picomolar affinities: Quantitative aspects of noncovalent and covalent binding of drugs to proteins. J Med Chem 52: 225-233, 2009.
75. Alqahtani S: In silico ADME-Tox modeling: Progress and prospects. Expert Opin Drug Metab Toxicol 13: 1147-1158, 2017.
76. Nandini Asha R, Ravindran Durai Nayagam B and Bhuvanesh N: Synthesis, molecular docking, and in silico ADMET studies of 4-benzyl-1-(2,4,6-trimethyl-benzyl)-piperidine: Potential inhibitor of SARS-CoV2. Bioorg Chem 112: 104967, 2021.
77. Almeleebia TM, Shahrani MA, Alshahrani MY, Ahmad I, Alkahtani AM, Alam MJ, Kausar MA, Saeed A, Saeed M and Iram S: Identification of new mycobacterium tuberculosis proteasome inhibitors using a knowledge-based computational screening approach. Molecules 26: 2326, 2021.
78. Gentile D, Floresta G, Patamia V, Chiaramonte R, Mauro GL, Rescifina A and Vecchio M: An integrated pharmacophore/Docking/3D-QSAR approach to screening a large library of products in search of future botulinum neurotoxin a inhibitors. Int J Mol Sci 21: 9470, 2020.
79. Daina A, Michielin O and Zoete V: SwissADME: A free web tool to evaluate pharmacokinetics, drug-likeness and medicinal chemistry friendliness of small molecules. Sci Rep 7: 42717, 2017.
80. Gfeller D, Grosdidier A, Wirth M, Daina A, Michielin O and Zoete V: SwissTargetPrediction: A web server for target prediction of bioactive small molecules. Nucleic Acids Res 42(Web Server Issue): W32-W38, 2014.
81. Abdelfatah S, Bockers M, Asensio M, Kadioglu O, Klinger A, Fleischer E and Efferth T: Isopetasin and S-isopetasin as novel P-glycoprotein inhibitors against multidrug-resistant cancer cells. Phytomedicine 86: 153196, 2021.
82. Greish KF, Salerno L, Al Zahrani R, Amata E, Modica MN, Romeo G, Marrazzo A, Prezzavento O, Sorrenti V, Rescifina A, *et al*: Novel structural insight into inhibitors of heme oxygenase-1 (HO-1) by new imidazole-based compounds: Biochemical and in vitro anticancer activity evaluation. Molecules 23: 1209, 2018.
83. Verma K, Kannan K, V S, R S, V K and K R: Exploring β-tubulin inhibitors from plant origin using computational approach. Phytochem Anal 28: 230-241, 2017.
84. Lo YC and Torres JZ: Chemical similarity networks for drug discovery. In: Special Topics in Drug Discovery. Chen T (ed). IntechOpen. Volume 1: 53-70, 2016.
85. Duran-Frigola M, Pauls E, Guitart-Pla O, Bertoni M, Alcalde V, Amat D, Juan-Blanco T and Aloy P: Extending the small-molecule similarity principle to all levels of biology with the Chemical Checker. Nat Biotechnol 38: 1087-1096, 2020.
86. Jasial S, Hu Y, Vogt M and Bajorath J: Activity-relevant similarity values for fingerprints and implications for similarity searching. F1000Res 5: Chem Inf Sci-591, 2016.
87. Kropiwnicki E, Evangelista JE, Stein DJ, Clarke DJB, Lachmann A, Kuleshov MV, Jeon M, Jagodnik KM and Ma'ayan A: Drugmonizome and Drugmonizome-ML: Integration and abstraction of small molecule attributes for drug enrichment analysis and machine learning. Database (Oxford) 2021: baab017, 2021.
88. Lambert LJ, Grotegut S, Celeridad M, Gosalia P, Backer LJ, Bobkov AA, Salaniwal S, Chung TD, Zeng FY, Pass I, *et al*: Development of a robust high-throughput screening platform for inhibitors of the striatal-enriched tyrosine phosphatase (STEP). Int J Mol Sci 22: 4417, 2021.
89. Lopez-Lopez E, Cerda-Garcia-Rojas CM and Medina-Franco JL: Tubulin inhibitors: A chemoinformatic analysis using cell-based data. Molecules 26: 2483, 2021.
90. Thomas M, Smith RT, O'Boyle NM, de Graaf C and Bender A: Comparison of structure- and ligand-based scoring functions for deep generative models: A GPCR case study. J Cheminform 13: 39, 2021.